Nonlinear Dyn (2015) 79:1727–1743
DOI 10.1007/s11071-014-1770-x

ORIGINAL PAPER

Unified nonlinear electroelastic dynamics of a bimorph piezoelectric cantilever for energy harvesting, sensing, and actuation

Stephen Leadenham · Alper Erturk

Received: 23 June 2014 / Accepted: 21 October 2014 / Published online: 6 November 2014

Abstract Inherent nonlinearities of piezoelectric materials are pronounced in various engineering applications such as sensing, actuation, combined applications for vibration control, and energy harvesting from dynamical systems. The existing literature focusing on the dynamics of electroelastic structures made of piezoelectric materials has explored such nonlinearities separately for the problems of mechanical and electrical excitation. Similar manifestations of softening nonlinearities have been attributed to purely elastic nonlinear terms, coupling nonlinearities, hysteresis alone, or a combination of these effects by various authors. In order to develop a unified nonlinear nonconservative framework with two-way coupling, the present work investigates the nonlinear dynamic behavior of a bimorph piezoelectric cantilever under low to moderately high mechanical and electrical excitation levels in energy harvesting, sensing, and actuation. The highest voltage levels, for near resonance investigation, are well below the coercive field. A distributed parameter electroelastic model is developed by accounting for softening and dissipative nonlinearities to analyze the primary resonance of a soft (e.g., PZT-5A, PZT-5H) piezoelectric cantilever for the fundamental bending mode using the method of harmonic balance. Excellent agreement between the model and experimental investigation is found, providing evidence that quadratic stiffness, damping, and electromechanical coupling effects accurately model predominantly observed nonlinear effects in geometrically linear vibration of piezoelectric cantilever beams. The backbone curves of both energy harvesting and actuation frequency responses for a PZT-5A cantilever are experimentally found to be dominantly of first order and specifically governed by ferroelastic quadratic softening for a broad range of mechanical and electrical excitation levels. Cubic and higher-order nonlinearities become effective only near the physical limits of the brittle and stiff (geometrically linear) bimorph cantilever when excited near resonance.

Keywords Piezoelectricity · Nonlinear analysis · Energy harvesting · Sensing · Actuation

S. Leadenham · A. Erturk (✉)
Georgia Institute of Technology, Atlanta, GA, USA
e-mail: alper.erturk@me.gatech.edu

1 Introduction

Nonlinearities of piezoelectric materials are manifested in various engineering applications such as sensing, actuation, as well as their combined applications for vibration damping and control, and most recently, energy harvesting from dynamical systems. Literature dealing with the dynamics of electroelastic structures made of piezoelectric materials has explored such nonlinearities in a disconnected way for the separate problems of mechanical and electrical excitation, such that nonlinear resonance trends have been assumed to be due to different additional terms in constitutive equations by different researchers. Similar patterns of softening nonlinearities have been attributed to purely elastic nonlinear terms, coupling nonlinearities, or both of these effects by various authors. After early investigation by Maugin [1] and Tiersten [2] into nonlinear electromechanical effects of piezoelectric materials, the nonlinear analysis of actuated piezoelectric beams started to gain momentum. Aurelle et al. [3] studied the contribution of strain and electromechanical coupling to the nonlinear response of an actuated beam under low electric field excitation with stress (T_1) modeled as,

$$T_1 = c_{11} S_1 - e_{31} E_3 + \alpha_{111} S_1^2 + \gamma_{311} S_1 E_3,$$

where S_1 is the strain, E_3 is the electric field, c_{11} and e_{31} represent the linear elastic and piezoelectric constants in the standard form [1], while α_{111} and γ_{311} are the nonlinear constants. Experimentally shown attenuations in amplitude beyond linear damping was attributed to the electromechanical coupling term γ_{311}. Guyomar et al. [4] justified the approach used by Aurelle et al. [3] by showing that a term proportional to the square of electric field was negligible. Recently, Abdelkefi et al. [5,6] used the constitutive equations suggested by Aurelle et al. [3] for nonlinear piezoelectric energy harvester modeling and simulations. Studying both weak and high electric fields, Wang et al. [7], showed how deviating from weak electric fields increased the effect of electromechanical nonlinearities through third-order elasticity and second-order electric field with a cross $S_1 E_3$ expression in the stress equation. This work also attributed high actuation level attenuation toward nonlinear damping dependent on the electric field. Albareda et al. [8] only considered higher-order elasticity nonlinearities in the formulation of the thermodynamic potential (free electric enthalpy density or the Gibbs free energy density). Priya et al. [9] analyzed high electric field nonlinear elastic and electromechanical nonlinearities, but found that the electromechanical terms depended on the square of the strain amplitude. Wolf and Gottlieb [10] also attributed the nonlinear phenomenon of an actuated cantilever in both symmetric (bimorph) and asymmetric (unimorph) configurations to elasticity by considering an electric enthalpy density of

$$H = \frac{1}{2} c_{11} S_1^2 - e_{31} E_3 S_1 - \frac{1}{2} \epsilon_{33} E_3^2 + \frac{1}{6} c_3 S_1^3 + \frac{1}{24} c_4 S_1^4,$$

which results in second- and third-order elastic dependence in the stress equation related to c_3 and c_4 (depending on the bimorph or unimorph arrangement, i.e., symmetry with respect to the reference surface) along with a linear dependence on electric field and electromechanical coupling. This model was experimentally applied by Usher et al. [11] Von Wagner and Hagedorn [12] derived an electric enthalpy density formula to take into account quadratic and cubic nonlinearities of strain and coupling. The resulting electric enthalpy density expression was

$$\begin{aligned} H = {} & \frac{1}{2} c_0 S_1^2 + \frac{1}{3} c_1 S_1^3 + \frac{1}{4} c_2 S_1^4 - \gamma_0 S_1 E_3 \\ & - \frac{1}{2} \gamma_1 S_1^2 E_3 - \frac{1}{3} \gamma_2 S_1^3 E_3 - \frac{1}{2} \nu_2 E_3^2, \end{aligned}$$

where c_1, c_2, γ_1, and γ_2 represent the nonlinear parameters. Also taking a purely geometric nonlinearity approach, Mahmoodi et al. [13] analyzed a MEMS piezoelectrically coupled cantilever. This was validated by assuming low electric field and that material nonlinearities due to strain were an order of magnitude larger than coupling parameters. The analysis shows the importance of the backbone curve, which tracks peak amplitude for increasing voltage excitation levels, in the identification of nonlinear parameters.

From this review of nonlinear actuation models, it is evident that a consistent approach has yet to be developed. Even in cases with weak electric field, it is unclear whether nonlinear electromechanical coupling can be excluded. Additionally, proper modeling is typically avoided when deriving the constitutive equation pair from a higher-order form of electric enthalpy. Further efforts are due to the analysis of the energy harvesting problem as summarized next.

Hu et al. [14] analyzed the nonlinear behavior of a shear vibration piezoelectric energy harvester by applying the cubic theory of the displacement gradient initially introduced by Maugin [1] and Tiersten [2]. Higher-order electromechanical coupling and electric field terms were neglected due to the weak electric field assumption. Stanton et al. [15,16] studied the results of higher order strain and electromechanical coupling and attributed experimentally shown peak attenuation at higher excitation levels to a nonlinear quadratic damping term [17]. Later, considering weak electric fields in energy harvesting, the same group [18] reanalyzed the energy harvesting problem by removing higher-order electromechanical coupling and considering only elastic nonlinearities up to fifth order,

$$T_1 = c_{11} S_1 - e_{31} E_3 + c_3 S_1^2 + c_4 S_1^3 + c_5 S_1^4 + c_6 S_1^5,$$

and this approach was suggested to be more consistent, since the electric field levels in energy harvesting are not as high as those in actuation. As an alternative to the aforementioned models developed by von Wagner [12] and Stanton et al. [15], Goldschmidtboeing et al. [19] recently explored the effect of ferroelastic (stress–strain) hysteresis on piezoelectric cantilever beams. This group chose to ignore higher-order nonlinear elasticity and nonlinear coupling terms, and instead attribute observed nonlinear effects entirely to hysteresis. This resulted in a constitutive equation of the form,

$$T_1 = c_{11} \left(1 - \alpha |S_1|\right) S_1 - e_{31} E_3,$$

and per cycle energy density dissipation relation,

$$U_{\mathrm{dis}} = \frac{4}{3} \gamma c_{11} |S_1|^3,$$

where $|S_1|$ is the strain amplitude, and α and γ are parameters quantifying the hysteretic softening and dissipation effects (not be confused with ferroelectric or dielectric hysteresis effects [20–22], since electric field levels in energy harvesting are well below the coercive field). The modeling of ferroelastic hysteresis [19] provided a single physical explanation for both the observed nonlinear stiffness and damping effects.

The discrepancy within and between the actuation and energy harvesting nonlinear analyses shows that a unified model of a piezoelectrically coupled beam that works for both problems of two-way coupling does not yet exist. A reliable nonlinear constitutive equation for a given piezoelectric material is expected to be rather unique and valid regardless of the application, e.g., actuation, sensing, or energy harvesting. A systematic approach focusing on the two-way coupling can result in a sound mathematical framework. To this end, the present work investigates the nonlinear dynamic behavior of a bimorph piezoelectric cantilever under low to moderately high mechanical and electrical excitation levels (yielding electric fields well below the coercive field) in energy harvesting, sensing, and actuation. Building on previous work, both hysteretic, elastic, and electromechanical coupling nonlinearities are considered. A mathematical framework is developed by using the method of harmonic balance and compared to experiments to identify the nonlinear system parameters and validate the proposed model for a broad range of mechanical and electrical excitation levels within the structural failure limits of a PZT-5A bimorph cantilever.

2 Nonlinear, nonconservative electroelastic modeling

The system to be studied consists of a symmetric piezoelectric bimorph cantilever with two piezoelectric layers on either side of a metal central layer. The piezoelectric layers are poled in the thickness direction, with the top and bottom surfaces forming the electrodes. A diagram of the bimorph for energy harvesting from base motion and dynamic actuation with fixed base is shown in Fig. 1 for the series and parallel connection cases of the piezoelectric layers. The cantilever used in this work exhibits high stiffness, resulting in small deflections and slopes for all practical excitation levels within the structural failure limits. This ensures that geometric nonlinearity is negligible, making observation and identification of the electroelastic nonlinearities of interest possible. Considering the work of von Wagner and Hagedorn [12] and Goldschmidtboeing et al. [19], the following nonlinear electric enthalpy density expression is proposed along with a nonlinear structural dissipation term:

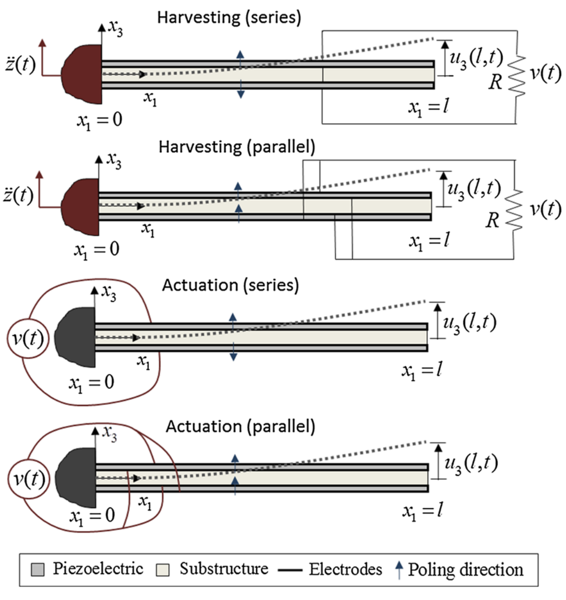

Fig. 1 Schematic representation of a piezoelectric bimorph for operation in base motion energy harvesting and actuation with series and parallel wiring configurations

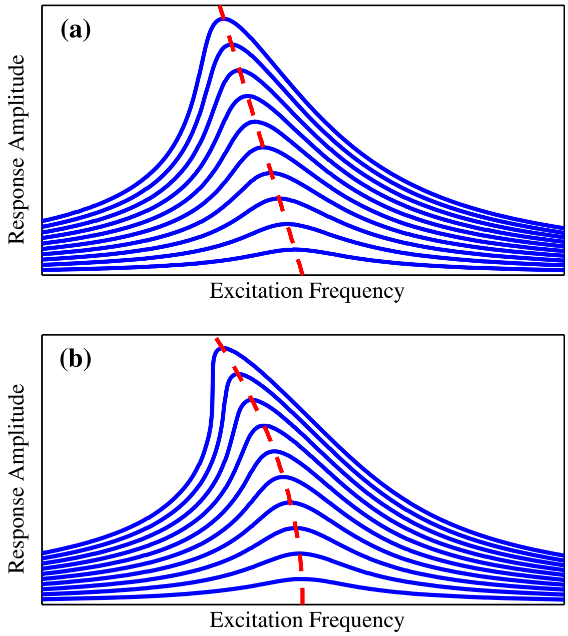

Fig. 2 Response of an oscillator with quadratic (**a**) and cubic (**b**) softening stiffness nonlinearity. Response curves at various excitation amplitudes are shown by *solid blue lines*. The backbone curve is shown by a *dashed red line*

$$H = \frac{1}{2}c_{11}S_1^2 + \frac{1}{3}c_{111}S_1^3\,\mathrm{sgn}(S_1) - e_{31}S_1E_3 - \frac{1}{2}e_{311}S_1^2\,\mathrm{sgn}(S_1)E_3 - \frac{1}{2}\epsilon_{33}E_3^2 \quad (1)$$

$$U_{\mathrm{dis}} \propto |S_1|^3. \quad (2)$$

As discussed previously, common practice currently is to express the enthalpy as a polynomial in the strain and electric field. When applying such a model to a symmetric structure, terms proportional to second-order nonlinear coefficients vanish, making third-order nonlinear terms necessary to predict any nonlinear behavior. In this work, an electric enthalpy density expressed as a polynomial in the strain magnitude, rather than the strain itself, is proposed. In this way, second-order terms do not vanish unlike the previous efforts [12,15]. For illustration, Fig. 2 shows behavior due to quadratic and cubic stiffness nonlinearities. While both quadratic and cubic stiffness models can exhibit the same type of nonlinearities (hardening or softening) as an experimentally observed system, the two models are qualitatively different. This is apparent by examining the *backbone curve*, which connects the peaks of frequency response curves at all excitation amplitudes. A quadratic stiffness model, e.g.,

$$\ddot{x} + 2\zeta\dot{x} + x - x^2\,\mathrm{sgn}(x) = f(t),$$

predicts a backbone curve that changes linearly with the response amplitude as in Fig. 2a. A cubic stiffness model, e.g.,

$$\ddot{x} + 2\zeta\dot{x} + x - x^3 = f(t),$$

predicts a quadratic variation of the peak response frequency with response amplitude as in Fig. 2b. As shown by Goldschmidtboeing et al. [19], stiff piezoelectric bimorphs display a linear decrease in peak response frequency with increased excitation level. In fact, other published experimental data in the literature also exhibit first-order backbone curve trends in soft piezoelectrics, e.g., Fig. 4 in Usher and Sim [11] and Fig. 5 in Mahmoodi et al. [13], among others, while the respective models predict second-order backbone curves. Therefore, a model is required that does not allow second-order stiffness and electromechanical coupling terms to vanish. As for nonlinear dissipation, only mechanical (ferroelastic) hysteresis is assumed with Eq. (2), since the present work is intended for low to moderate excitation levels near resonance, yielding electric fields well below of the coercive field of piezoelectric layers. Therefore, ferroelectric (polarization electric field) and dielectric (electric displacement field) hysteresis effects [21] and resulting high-field losses are excluded in this framework.

3 Distributed parameter model derivation

From the electric enthalpy density expression, the longitudinal stress, T_1, and the transverse electric displacement, D_3, can be found using the following relations:

$$T_1 = \frac{\partial H}{\partial S_1},\ D_3 = -\frac{\partial H}{\partial E_3}, \quad (3)$$

yielding,

$$T_1 = c_{11}S_1 + c_{111}S_1^2\,\mathrm{sgn}(S_1) - e_{31}E_3 - e_{311}S_1\,\mathrm{sgn}(S_1)E_3 \quad (4)$$

$$D_3 = e_{31}S_1 + \frac{1}{2}e_{311}S_1^2\,\mathrm{sgn}(S_1) + \epsilon_{33}E_3, \quad (5)$$

which satisfy,

$$\frac{\partial T_1}{\partial E_3} = -\frac{\partial D_3}{\partial S_1}. \quad (6)$$

Deformations are assumed to be small (in agreement with the experiments for the stiff and brittle sample explored in this work); therefore, axial strain in the beam is modeled using Euler–Bernoulli theory, namely

$$S_1 = -x_3 u_3''(x_1, t), \tag{7}$$

where $u_3(x_1, t)$ is the transverse deflection of the beam from equilibrium, and $(\,)'$ denotes the spatial derivative, $\partial/\partial x_1$. For the case of series connected piezoelectric laminates, the transverse electric field is modeled as

$$E_3 = -\frac{\dot{\lambda}}{2h_\mathrm{p}}\,\mathrm{sgn}(x_3), \tag{8}$$

where λ is a electric flux linkage coordinate [15,18,23], h_p is the thickness of each piezoelectric layer, and $\dot{(\,)}$ denotes the time derivative, $\partial/\partial t$. The time derivative of flux linkage represents the electrode voltage, which will be substituted in later in the analysis. For the case of parallel connected electrodes, the electric field is modeled as

$$E_3 = -\frac{\dot{\lambda}}{h_\mathrm{p}}\,\mathrm{sgn}(x_3). \tag{9}$$

The total kinetic energy of the beam undergoing prescribed transverse base motion is,

$$T = \frac{1}{2}\int_0^l \hat{m}\big[\dot{u}_3 + \dot{z}(t)\big]^2 \mathrm{d}x_1. \tag{10}$$

The base velocity is denoted by $\dot{z}(t)$, and $\hat{m}$ represents the mass per unit length of the bimorph. The total potential energy of the piezoelectric bimorph is the sum of the potential energies of the substrate, U_s, and piezoelectric laminates, U_p:

$$U = U_\mathrm{s} + U_\mathrm{p}. \tag{11}$$

The substrate strain energy can be expressed as,

$$U_\mathrm{s} = \frac{1}{2}\int_0^l \frac{c_\mathrm{s} b h_\mathrm{s}^3}{12}\left(u_3''\right)^2 \mathrm{d}x_1, \tag{12}$$

where c_s is the substrate Young's modulus, b is the width of the beam, and h_s is the thickness of the substrate layer. The piezoelectric laminate potential energy is volumetric integral of the electric enthalpy density, H.

$$U_\mathrm{p} = \int_{V_\mathrm{p}} H\,\mathrm{d}V_\mathrm{p} = \int_0^l \left\{\int_{-\frac{b}{2}}^{\frac{b}{2}}\left[\int_{\frac{h_\mathrm{s}}{2}}^{\frac{h_\mathrm{s}}{2}+h_\mathrm{p}} H\,\mathrm{d}x_3 + \int_{-\frac{h_\mathrm{s}}{2}-h_\mathrm{p}}^{-\frac{h_\mathrm{s}}{2}} H\,\mathrm{d}x_3\right]\mathrm{d}x_2\right\}\mathrm{d}x_1 \tag{13}$$

Performing the spatial integration over the cross section yields the following potential energy expression:

$$U = \frac{1}{2}\int_0^l \left\{\hat{k}_1\left(u_3''\right)^2 + \frac{1}{3}\hat{k}_2\left(u_3''\right)^3 \mathrm{sgn}(u_3'') - \left[2\hat{\theta}_1 u_3'' + \hat{\theta}_2\left(u_3''\right)^2 \mathrm{sgn}(u_3'')\right]\dot{\lambda}\right\}\mathrm{d}x_1 - \frac{1}{2}C\dot{\lambda}^2 \tag{14}$$

The distributed mass and stiffness coefficients are given as:

$$\begin{aligned}
\hat{m} &= b(\rho_\mathrm{s} h_\mathrm{s} + 2\rho_\mathrm{p} h_\mathrm{p})\\
\hat{k}_1 &= \frac{1}{12}c_\mathrm{s} b h_\mathrm{s}^3 + \frac{1}{6}c_{11} b h_\mathrm{p}\left(4h_\mathrm{p}^2 + 6h_\mathrm{p}h_\mathrm{s} + 3h_\mathrm{s}^2\right)\\
\hat{k}_2 &= \frac{1}{2}c_{111} b h_\mathrm{p}\left(2h_\mathrm{p}^3 + 4h_\mathrm{p}^2 h_\mathrm{s} + 3h_\mathrm{p}h_\mathrm{s}^2 + h_\mathrm{s}^3\right)
\end{aligned} \tag{15}$$

For series connected electrodes, the electromechanical coupling coefficients and harvester capacitance are

$$\begin{aligned}
\hat{\theta}_1 &= \frac{1}{2}e_{31} b\left(h_\mathrm{p} + h_\mathrm{s}\right)\\
\hat{\theta}_2 &= \frac{1}{12}e_{311} b\left(4h_\mathrm{p}^2 + 6h_\mathrm{p}h_\mathrm{s} + 3h_\mathrm{s}^2\right)\\
C &= \frac{b l^* \epsilon_{33}}{2h_\mathrm{p}}.
\end{aligned} \tag{16}$$

For parallel connected electrodes, the electromechanical coupling coefficients and harvester capacitance are

$$\begin{aligned}
\hat{\theta}_1 &= e_{31} b\left(h_\mathrm{p} + h_\mathrm{s}\right)\\
\hat{\theta}_2 &= \frac{1}{6}e_{311} b\left(4h_\mathrm{p}^2 + 6h_\mathrm{p}h_\mathrm{s} + 3h_\mathrm{s}^2\right)\\
C &= \frac{2b l^* \epsilon_{33}}{h_\mathrm{p}}.
\end{aligned} \tag{17}$$

In both series and parallel connected electrode cases, the capacitance, C, depends on the effective length of the bimorph, l^*, rather than the overhanging cantilever length, l. In this work, the total length is used for l^*.

To generate governing partial differential equations and boundary conditions, Hamilton's principle is used.

$$\int_{t_0}^{t_1}\left(\delta L + \delta W_\mathrm{nc}\right)\mathrm{d}t = 0 \tag{18}$$

The Lagrangian, L, is the difference of kinetic and potential energy, $T - U$, and δW_nc is the nonconservative virtual work. The variation of the Lagrangian can be expressed using the chain rule,

$$\delta L\left(\dot{u}_3, u_3'', \dot{\lambda}\right) = \frac{\partial L}{\partial \dot{u}_3}\delta\dot{u}_3 + \frac{\partial L}{\partial \dot{\lambda}}\delta\dot{\lambda} + \frac{\partial L}{\partial u_3''}\delta u_3''. \quad (19)$$

The nonconservative virtual work is comprised of three parts: first-order structural damping, second-order structural damping due to Eq. (2), and dissipation due to Joule heating of the load resistance.

$$\delta W_{\mathrm{nc}} = -\int_0^l \left[\hat{b}_1 u_3 \operatorname{sgn}(u_3) + \hat{b}_2 u_3^2\right] \times \operatorname{sgn}(\dot{u}_3)\delta u_3 \mathrm{d}x_1 - \frac{\dot{\lambda}}{R}\delta\lambda \quad (20)$$

Integrating by parts results in a variational expression for the governing partial differential equations and boundary conditions.

$$\int_{t_0}^{t_1}\Bigg\{\Bigg[-\frac{\partial}{\partial t}\left(\frac{\partial L}{\partial \dot{u}_3}\right) + \frac{\partial^2}{\partial x_1^2}\left(\frac{\partial L}{\partial u_3''}\right) - \int_0^l \left[\hat{b}_1 u_3 \operatorname{sgn}(u_3) + \hat{b}_2 u_3^2\right]\operatorname{sgn}(\dot{u}_3)\mathrm{d}x_1\Bigg]\delta u_3 + \left[-\frac{\partial}{\partial t}\left(\frac{\partial L}{\partial \dot{\lambda}}\right) - \frac{\dot{\lambda}}{R}\right]\delta\lambda + \left[-\frac{\partial}{\partial x_1}\left(\frac{\partial L}{\partial u_3''}\right)\right]\delta u_3\big|_0^l + \frac{\partial L}{\partial u_3''}\delta u_3'\big|_0^l\Bigg\}\mathrm{d}t = 0 \quad (21)$$

The first portion governs the mechanical domain for arbitrary δu_3:

$$-\frac{\partial}{\partial t}\left(\frac{\partial L}{\partial \dot{u}_3}\right) + \frac{\partial^2}{\partial x_1^2}\left(\frac{\partial L}{\partial u_3''}\right) - \int_0^l \left[\hat{b}_1 u_3 \operatorname{sgn}(u_3) + \hat{b}_2 u_3^2\right]\operatorname{sgn}(\dot{u}_3)\mathrm{d}x_1 = 0, \quad (22)$$

and results in the PDE:

$$\hat{m}\ddot{u}_3 + \left(\hat{b}_1 u_3 \operatorname{sgn}(u_3) + \hat{b}_2 u_3^2\right)\operatorname{sgn}(\dot{u}_3) + \hat{k}_1 u_3^{(4)} + \hat{k}_2\left[u_3'' u_3^{(4)} + \left(u_3^{(3)}\right)^2\right]\operatorname{sgn}(u_3'') - \left\{\hat{\theta}_1\left[\delta'(x_1) - \delta'(x_1 - l)\right] + \hat{\theta}_2 u_3^{(4)}\operatorname{sgn}(u_3'')\right\}\dot{\lambda} = -\hat{m}\ddot{z}(t). \quad (23)$$

Here, δ' represents the first spatial derivative of the Dirac delta function. The second portion of the variational expression for arbitrary $\delta\lambda$ governs the electrical domain:

$$-\frac{\partial}{\partial t}\left(\frac{\partial L}{\partial \dot{\lambda}}\right) - \frac{\dot{\lambda}}{R} = 0, \quad (24)$$

and results in the ODE:

$$C\ddot{\lambda} + \frac{\dot{\lambda}}{R} + \int_0^l \left[\hat{\theta}_1 + \hat{\theta}_2 u_3'' \operatorname{sgn}(u_3'')\right]\dot{u}_3''\mathrm{d}x_1 = 0. \quad (25)$$

Substituting voltage, v, for the time derivative of the flux linkage coordinate, λ, yields the following pair of governing differential equations for the piezoelectric bimorph:

$$\hat{m}\ddot{u}_3 + \left(\hat{b}_1 u_3 \operatorname{sgn}(u_3) + \hat{b}_2 u_3^2\right)\operatorname{sgn}(\dot{u}_3) + \hat{k}_1 u_3^{(4)} + \hat{k}_2\left[u_3'' u_3^{(4)} + \left(u_3^{(3)}\right)^2\right]\operatorname{sgn}(u_3'') - \left\{\hat{\theta}_1\left[\delta'(x_1) - \delta'(x_1 - l)\right] + \hat{\theta}_2 u_3^{(4)}\operatorname{sgn}(u_3'')\right\}v = -\hat{m}\ddot{z}(t) \quad (26)$$

$$C\dot{v} + \frac{v}{R} + \int_0^l \left[\hat{\theta}_1 + \hat{\theta}_2 u_3'' \operatorname{sgn}(u_3'')\right]\dot{u}_3''\mathrm{d}x_1 = 0. \quad (27)$$

4 Discretization

To reduce the partial differential equations to ordinary differential equations, Galerkin's method is applied. A single-mode solution is used for the first bending mode, namely

$$u_3(x_1, t) = x(t)\phi(x_1). \quad (28)$$

Here, $x(t) = u_3(l, t)$ is the deflection of the cantilever tip relative to equilibrium, and $\phi(x_1)$ is the unit normalized shape function, i.e.,

$$\phi(l) = 1. \quad (29)$$

Substitution of Eq. (28) into Eq. (26), multiplying by $\phi(x_1)$, and integrating over the length, yields the following ordinary differential equation for the mechanical behavior of the bimorph,

$$m\ddot{x} + \left(b_1 x \operatorname{sgn}(x) + b_2 x^2\right)\operatorname{sgn}(\dot{x}) + k_1 x + k_2 x^2 \operatorname{sgn}(x) - \left[\theta_1 + \theta_2 x \operatorname{sgn}(x)\right]v = -\bar{m}\ddot{z}(t). \quad (30)$$

Substitution of Eq. (28) into Eq. (27) results in the governing equation for the electrical behavior of the bimorph,

$$C\dot{v} + \frac{v}{R} + \left[\theta_1 + \psi_2 x \,\mathrm{sgn}(x)\right]\dot{x} = 0. \tag{31}$$

The spatially discretized model is parameterized by the following values:

$$\begin{aligned}
m &= \hat{m}\int_0^l \phi^2 \mathrm{d}x_1 \\
\bar{m} &= \hat{m}\int_0^l \phi \,\mathrm{d}x_1 \\
b_1 &= \hat{b}_1\int_0^l \phi^2 \mathrm{d}x_1 \\
b_2 &= \hat{b}_2\int_0^l \phi^3 \,\mathrm{sgn}(\phi)\mathrm{d}x_1 \\
k_1 &= \hat{k}_1\int_0^l \phi^{(4)}\phi \,\mathrm{d}x_1 \\
k_2 &= \hat{k}_2\int_0^l \left[\phi''\phi^{(4)} + \left(\phi^{(3)}\right)^2\right]\phi \,\mathrm{sgn}(\phi'')\mathrm{d}x_1 \\
\theta_1 &= \hat{\theta}_1\phi'(l) \\
\theta_2 &= \hat{\theta}_2\int_0^l \phi^{(4)}\phi \,\mathrm{sgn}(\phi'')\mathrm{d}x_1 \\
\psi_2 &= \hat{\theta}_2\int_0^l \left(\phi''\right)^2 \mathrm{sgn}(\phi'')\mathrm{d}x_1.
\end{aligned} \tag{32}$$

In this analysis, the first mode shape of a purely mechanical Euler–Bernoulli cantilever beam is chosen for ϕ, i.e.,

$$\begin{aligned}
\phi(x_1) = \frac{1}{2}\Bigg\{&\cosh\left(\frac{\beta x_1}{l}\right) - \cos\left(\frac{\beta x_1}{l}\right) \\
&-\sigma\left[\sinh\left(\frac{\beta x_1}{l}\right) - \sin\left(\frac{\beta x_1}{l}\right)\right]\Bigg\},
\end{aligned} \tag{33}$$

with

$$\begin{aligned}
\beta &= 1.87510407 \\
\sigma &= 0.7341.
\end{aligned} \tag{34}$$

With this choice of ϕ, the forward and backward quadratic electromechanical coupling coefficients, θ_2 and ψ_2 are equal, similar to the result shown by Stanton et al. [15]

$$\theta_2 = \psi_2 \tag{35}$$

4.1 Energy harvesting and sensing

For the case of energy harvesting and sensing, the bimorph is subjected to a transverse base acceleration, $\ddot{z}(t)$, and the electrodes are shunted by a load resistance, R. The lumped parameter dynamical model for energy harvesting is represented as,

$$\begin{aligned}
&m\ddot{x} + \left(b_1 x \,\mathrm{sgn}(x) + b_2 x^2\right)\mathrm{sgn}(\dot{x}) + k_1 x \\
&\quad + k_2 x^2 \,\mathrm{sgn}(x) - \left[\theta_1 + \theta_2 x \,\mathrm{sgn}(x)\right]v = -\bar{m}\ddot{z}(t)
\end{aligned} \tag{36}$$

$$C\dot{v} + \frac{v}{R} + \left[\theta_1 + \theta_2 x \,\mathrm{sgn}(x)\right]\dot{x} = 0. \tag{37}$$

The coordinates, x and v, are the relative tip displacement of the cantilever and the voltage across the electrodes. Here, $\bar{m}$ and m are base acceleration forcing constant and the effective mass of the beam. The parameters, b_1, k_1, and θ_1, are the linear damping, stiffness, and electromechanical coupling constants, respectively. The parameters k_2, b_2, and θ_2 represent the nonlinear stiffness, damping, and electromechanical coupling effects. The equivalent capacitance, C, is the value measured across the electrodes of the bimorph.

4.2 Dynamic actuation

The dynamic actuation case refers to the piezolectric bimorph fixed from one end to a rigid base and a prescribed dynamic voltage, $v(t)$, applied to the electrodes. The lumped parameter dynamical model for dynamic actuation is represented as,

$$\begin{aligned}
&m\ddot{x} + \left(b_1 x \,\mathrm{sgn}(x) + b_2 x^2\right)\mathrm{sgn}(\dot{x}) \\
&\quad + k_1 x + k_2 x^2 \,\mathrm{sgn}(x) = \left[\theta_1 + \theta_2 x \,\mathrm{sgn}(x)\right]v(t)
\end{aligned} \tag{38}$$

$$C\dot{v} + i + \left[\theta_1 + \theta_2 x \,\mathrm{sgn}(x)\right]\dot{x} = 0. \tag{39}$$

The model differs from the energy harvesting case in that the electromechanical coupling is now the forcing term on the right-hand side of Eq. (38), and the current through the bimorph, i, is supplied by the power source, rather than related to the voltage across the load resistance by Ohm's Law. The model parameters are the same as in Sect. 4.1, making Eqs. (36–39) a global set of nonlinear nonconservative equations in physical coordinates for energy harvesting, sensing, and dynamic actuation for geometrically linear deformations.

5 Harmonic balance analysis

The method of harmonic balance has been used extensively to analyze periodic solutions of nonlinear ordinary differential equations. A Fourier series solution is assumed, replacing the ordinary differential equations with algebraic equations. The error of the approximate solution is minimized in the Galerkin method sense. The resulting system of algebraic equations is solved iteratively, with a method such as the Newton-Raphson method. In this analysis, a single-term harmonic balance solution is sufficient to approximate the steady-state response to harmonic excitation.

5.1 Energy harvesting and sensing

For the energy harvesting and sensing configuration, base acceleration is taken to be harmonic with constant amplitude, i.e.,

$$\ddot{z}(t) = A\cos(\Omega t) \tag{40}$$

The unknown steady-state tip displacement and voltage responses are assumed to be of the form:

$$\begin{aligned} x(t) &= X_1\cos(\Omega t) + X_2\sin(\Omega t) \\ v(t) &= V_1\cos(\Omega t) + V_2\sin(\Omega t) \end{aligned} \tag{41}$$

The amplitude of x is given by $X = \sqrt{X_1^2 + X_2^2}$. Substitution of Eqs. (40) and (41) into Eqs. (36) and (37) and application of the harmonic balance method yields the following set of algebraic equations in X_1, X_2, V_1, and V_2:

$$\begin{aligned} &-m\Omega^2 X_1 + \left(\frac{2}{\pi}b_1 + \frac{4}{3\pi}b_2 X\right)X_2 \\ &\quad + \left(k_1 + \frac{8}{3\pi}k_2 X\right)X_1 - \theta_1 V_1 \\ &\quad - \frac{4}{3\pi}\theta_2\left[\frac{\left(2X_1^2 + X_2^2\right)V_1 + X_1 X_2 V_2}{X}\right] \\ &\quad + \bar{m}A = 0 \\ &-m\Omega^2 X_2 - \left(\frac{2}{\pi}b_1 + \frac{4}{3\pi}b_2 X\right)X_1 \\ &\quad + \left(k_1 + \frac{8}{3\pi}k_2 X\right)X_2 - \theta_1 V_2 \\ &\quad - \frac{4}{3\pi}\theta_2\left[\frac{X_1 X_2 V_1 + \left(X_1^2 + 2X_2^2\right)V_2}{X}\right] = 0 \\ &C\Omega V_2 + \frac{1}{R}V_1 + \left(\theta_1 + \frac{4}{3\pi}\theta_2 X\right)\Omega X_2 = 0 \\ &C\Omega V_1 - \frac{1}{R}V_2 + \left(\theta_1 + \frac{4}{3\pi}\theta_2 X\right)\Omega X_1 = 0. \end{aligned} \tag{42}$$

5.2 Dynamic actuation

For the dynamic actuation configuration, the unknown steady-state tip displacement is the same as in Eq. (41), while the voltage is replaced by the expression:

$$v(t) = V\cos(\Omega t). \tag{43}$$

The current flow through the piezoelectric bimorph is assumed to be of the form:

$$i(t) = I_1\cos(\Omega t) + I_2\sin(\Omega t). \tag{44}$$

Substituting Eqs. (43) and (44) into Eqs. (38) and (39) and application of the harmonic balance method yields the follow set of algebraic equations in X_1, X_2, I_1, and I_2:

$$\begin{aligned} &-m\Omega^2 X_1 + \left(\frac{2}{\pi}b_1 + \frac{4}{3\pi}b_2 X\right)X_2 \\ &\quad + \left(k_1 + \frac{8}{3\pi}k_2 X\right)X_1 \\ &\quad - \left[\theta_1 + \frac{4}{3\pi}\theta_2\left(\frac{2X_1^2 + X_2^2}{X}\right)\right]V = 0 \\ &-m\Omega^2 X_2 - \left(\frac{2}{\pi}b_1 + \frac{4}{3\pi}b_2 X\right)X_1 \\ &\quad + \left(k_1 + \frac{8}{3\pi}k_2 X\right)X_2 \\ &\quad - \frac{4}{3\pi}\theta_2\left(\frac{X_1 X_2}{X}\right)V = 0 \\ &I_1 + \left(\theta_1 + \frac{4}{3\pi}\theta_2 X\right)\Omega X_2 = 0 \\ &-I_2 + \left(\theta_1 + \frac{4}{3\pi}\theta_2 X\right)\Omega X_1 + C\Omega V = 0. \end{aligned} \tag{45}$$

5.3 Quasi-static actuation

Low-frequency harmonic actuation can be analyzed simply by setting the forcing frequency, Ω, equal to zero in Eq. (45) yielding,

$$\begin{aligned} &\left(\frac{2}{\pi}b_1 + \frac{4}{3\pi}b_2 X\right)X_2 + \left(k_1 + \frac{8}{3\pi}k_2 X\right)X_1 \\ &\quad - \left[\theta_1 + \frac{4}{3\pi}\theta_2\left(\frac{2X_1^2 + X_2^2}{X}\right)\right]V = 0 \\ &\quad - \left(\frac{2}{\pi}b_1 + \frac{4}{3\pi}b_2 X\right)X_1 + \left(k_1 + \frac{8}{3\pi}k_2 X\right)X_2 \\ &\quad - \frac{4}{3\pi}\theta_2\left(\frac{X_1 X_2}{X}\right)V = 0. \end{aligned} \tag{46}$$

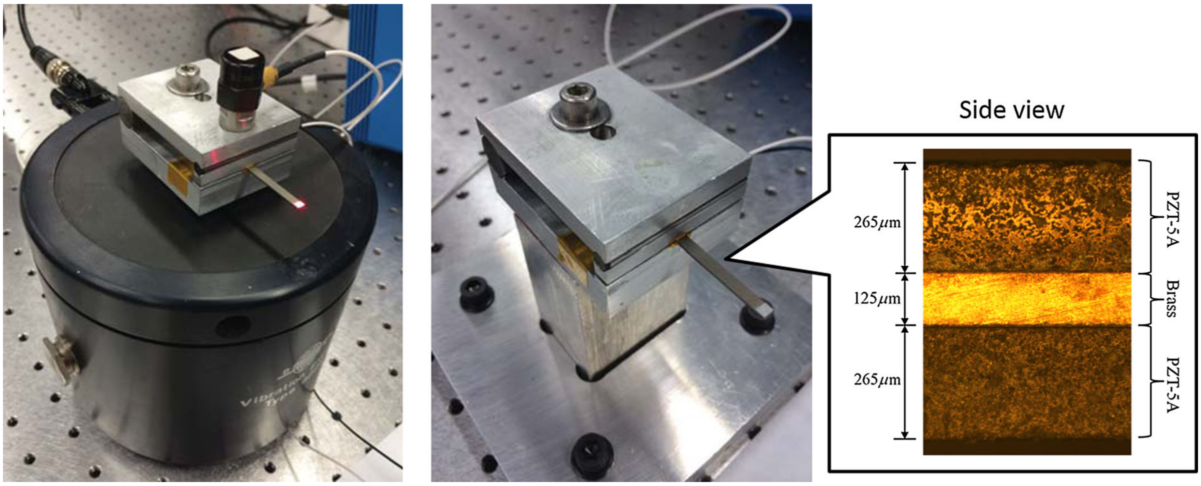

Fig. 3 Sample cantilever in fixture mounted to shaker for energy harvesting tests under base excitation (*left*) and mounted rigidly to table for dynamic actuation tests (*right*). In the *left* photograph, the accelerometer used for feedback control of the base acceleration is shown. A magnified side view of the bimorph shows the piezoelectric and brass substrate layers

6 Experimental validation

To validate the proposed model with quadratic nonlinearities in stiffness, damping, and electromechanical coupling, energy harvesting and dynamic actuation experiments are conducted.

6.1 Experimental setup

The test sample for the energy harvesting and dynamic actuation tests consists of a brass-reinforced PZT-5A piezoelectric cantilever bimorph (a Piezo Systems, Inc. T226-A4-103X with PZT-5A layers connected in series) secured in a custom fixture, shown in Fig. 3. Geometric and material properties of the bimorph can be found in Table 1 (the linear material parameters are in agreement with standard PZT-5A data [24] and manufacturer's data). For base excitation during energy harvesting tests, the fixture is mounted to a shaker (Brüel and Kjær Type 4809). Forward and reverse frequency sweeps at constant base acceleration amplitude are conducted using a vibration control system (APS Dynamics, Inc. VCS201) and accelerometer for acceleration feedback (Kistler AG Type 8636C5). The voltage across the cantilever electrodes are shunted across a load resistance box (IET Labs, Inc. RS-201W). Tip velocity measurements are made using a laser Doppler vibrometer (Polytec, Inc. OFV-505) and controller (Polytec, Inc. OFV-5000). Data is collected using National Instruments NI 9215 and NI 9223 data acquisition units. A schematic representation of the experimental setup is shown in Fig. 4.

Table 1 Material and geometric parameters

Overhang length	l	26.7	mm
Total length	l^*	31.8	mm
Width	b	3.16	mm
PZT-5A layer thickness (each)	h_p	0.265	mm
Brass layer thickness	h_s	0.125	mm
PZT-5A density	ρ_p	7,800	kg
PZT-5A linear stiffness	c_{11}	66	GPa
PZT-5A nonlinear stiffness	c_{111}	−60	TPa
PZT-5A linear coupling	e_{31}	−11.6	C/m^2
PZT-5A nonlinear coupling	e_{311}	−20	kC/m^2
Permittivity	ϵ_{33}	14.6	nF/m
Brass density	ρ_s	8,500	kg
Brass stiffness	c_s	100	GPa

During dynamic actuation experiments, the fixture is mounted to a rigid support. The actuation voltage signal is generated by a National Instruments NI USB-4431 and amplified using a power amplifier (Trek, Inc. Model 2220). Output voltage and current data are collected from the amplifier, as well as tip velocity measurements from the laser Doppler vibrometer and recorded using the NI USB-4431. A schematic representation of the experimental setup is shown in Fig. 5.

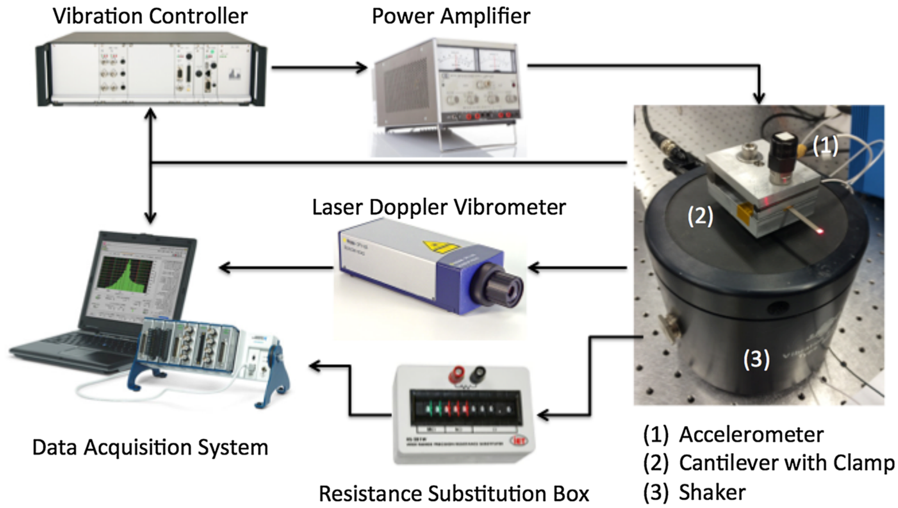

Fig. 4 Energy harvesting experimental apparatus

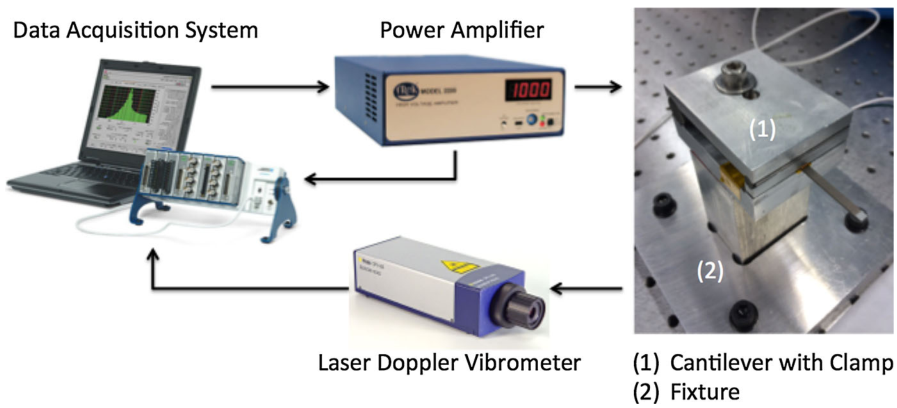

Fig. 5 Dynamic actuation experimental apparatus

6.2 Energy harvesting experiments and model validation

Energy harvesting experiments consist of frequency sweep tests at seven constant acceleration levels ranging from 0.01 g RMS to 1.0 g RMS. Tests at each acceleration level were repeated for nine load resistance values ranging from $1k\Omega$ to $10\,\mathrm{M}\Omega$, which cover a broad range between short- and open-circuit conditions. The upper limit for the base acceleration level results in a tip displacement approximately 60 % of the maximum allowable tip displacement given by the manufacturer. The tests therefore span nearly the entire safe operation limits for the cantilever bimorph. Figures 6, 7 and 8 display the RMS tip velocity and RMS voltage for the cantilever for different base acceleration and load resistance levels. The remaining results of energy harvesting experiments and modeled behavior is shown in the "Appendix". The identified model parameters are summarized in Table 2, from which the nonlinear elastic ($c_{111} = -60$ TPa) and piezoelectric ($e_{311} = -20\,\mathrm{kC/m^2}$) constants are extracted (Table 1).

As shown in Fig. 6, the model and experiment show excellent correlation at a low base acceleration level, where linear behavior is expected. The model and experiment only disagree for the voltage curves, when the harvester voltage is below the noise floor of the data acquisition unit, which is an experimental limitation. Agreement of the model and experiment in the linear behavior regime is important, but expected, as high-fidelity models for the linear behavior of piezoelectric cantilevers are readily available [24–26] to predict the linear electroelastic dynamics using the relevant geometric and material properties in Table 1.

Nonlinear behavior begins to appear at base acceleration levels as low as 0.05 g RMS and is readily apparent at 0.1 g RMS, as shown in Fig. 7. The short- and open-circuit resonant frequencies drop from 428 and

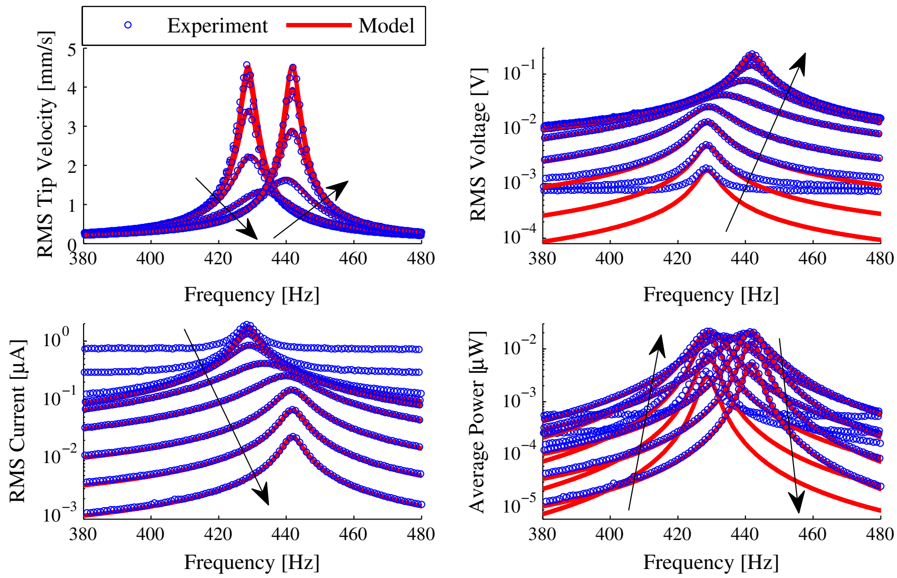

Fig. 6 Resistor sweep energy harvesting test at 0.01 g RMS base acceleration level for resistance values of 1, 3, 10, 30, 100, 300, 1, 3, and 10 MΩ. *Blue circles* represent experimental data, and red curves represent model predictions. *Arrows* indicate direction of increasing load resistance

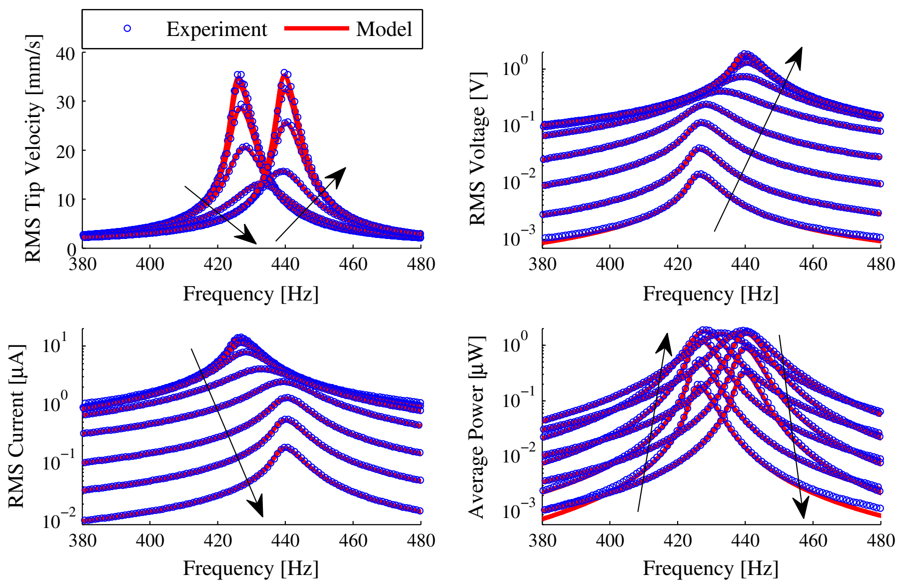

Fig. 7 Resistor sweep energy harvesting test at 0.1 g RMS base acceleration level for resistance values of 1, 3, 10, 30, 100, 300, 1, 3, and 10 MΩ. *Blue circles* represent experimental data, and *red curves* represent model predictions. *Arrows* indicate direction of increasing load resistance

442 Hz to 426 and 440 Hz respectively. Similarly, an increase in damping is observed as an order of magnitude increase in base acceleration results in a less than an order of magnitude increase in the responses. At 1g RMS base acceleration (Fig. 8) the trend continues, with the short- and open-circuit resonant frequencies falling to 415 and 430 Hz respectively, with increased damping. Note that the maximum tip vibration amplitude in the base excitation experiments is approximately 90 μm or 0.3 % of the overhang length. Therefore, the deformations are indeed geometrically linear, and nonlinearities can be attributed to material behavior. The early appearance of a softening nonlinear behavior and its near linear increase with excitation level is evidence that a negative cubic stiffness alone improperly models the type of softening present in this class of piezoelectric cantilevers. A cubic stiffness nonlinearity yields a frequency correction that rises quadratically with response amplitude, whereas ferroelastic softening and dissipation provides a physical mechanism for the observed linear frequency correction and damping increase. The electromechanical coupling nonlinearity causes an additional resonant frequency shift that increases from short- to open-circuit

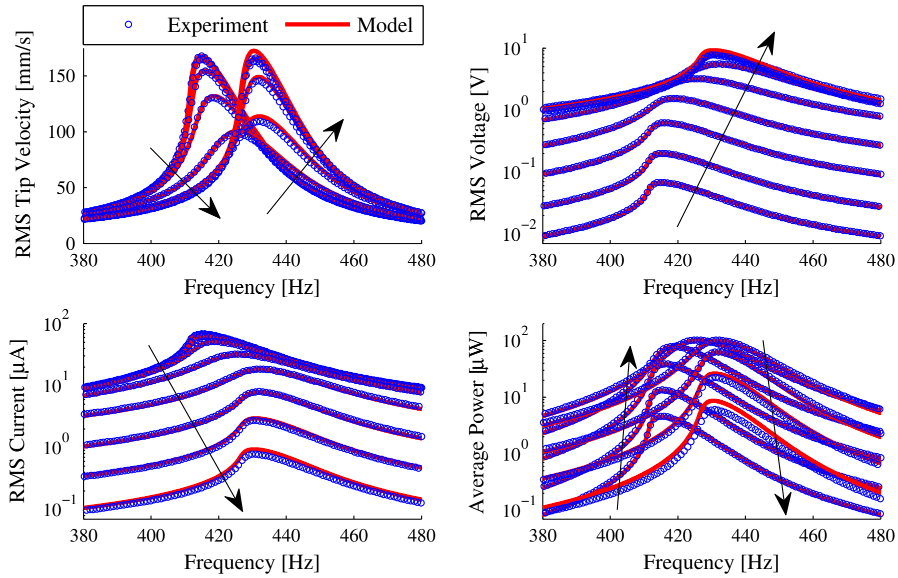

Fig. 8 Resistor sweep energy harvesting test at 1.0 g RMS base acceleration level for resistance values of 1, 3, 10, 30, 100, 300, 1, 3, and 10 MΩ. *Blue circles* represent experimental data, and *red curves* represent model predictions. *Arrows* indicate direction of increasing load resistance

Table 2 Discretized model parameters

Forcing mass	$\bar{m}$	1.72e−4	kg
Effective mass	m	1.10e−4	kg
Linear dissipation	b_1	1.40e1	N/m
Nonlinear dissipation	b_2	4.00e5	N/m^2
Linear stiffness	k_1	7.96e2	N/m
Nonlinear stiffness	k_2	−6.44e5	N/m^2
Linear coupling	θ_1	−3.69e−4	N/V
Nonlinear coupling	θ_2	−4.50e−1	N/Vm
Capacitance	C	2.76e−9	F

conditions (low to high voltage). Importantly, the proposed model shows very strong agreement at the low, medium, and high base acceleration levels.

6.3 Dynamic actuation experiments and model validation

Dynamic actuation tests are performed for voltages ranging from 0.01 to 10 V and shown in Fig. 9. This captures both the low voltage linear behavior and higher voltage behavior near the structural safety limits of the cantilever. These voltage levels result in electric fields well below the coercive field ($E_c = 12$ kV/cm for PZT-5A according to the manufacturer). However, resonant actuation above 10 V amplitude in cantilever configuration is expected to result in mechanical failure of the stiff and brittle sample. Once again, the maximum tip vibration measured in the actuation experiments is approximately 120 μm or 0.4 % of the overhang length, confirming that the observed nonlinearities are due to the material. The model uses the same parameters as shown in Table 2. The model and experiment show strong agreement over the entire voltage range, except in the cases where the consumed current is below the noise floor of the amplifier's current monitor output. Between the low (0.01 V) and moderate (10 V) voltage actuation tests, the bimorph displayed a decrease in resonant frequency from 429 to 413 Hz, matching the behavior shown during the energy harvesting tests at short-circuit conditions. This is expected, because power amplifiers typically have very low output impedance, and the velocity response amplitudes for the corresponding dynamic actuation and energy harvesting experiments are of the same order of magnitude. As shown in Eq. (38), during dynamic actuation, the electromechanical coupling nonlinearity appears as a correction to the forcing amplitude. At moderate response amplitudes, this can appear to have the same effect as another quadratic dissipation effect,[1] making identification of the two parameters from the dynamic actuation tests alone difficult. However, as shown in Sect. 6.2, both effects are pronounced during the energy harvesting tests. The proposed model for dynamic actu-

[1] A set of actuation experiments conducted in vacuum (not reported here) yield almost identical frequency response curves, suggesting that the quadratic dissipation is an internal nonlinear loss rather than due to air damping.

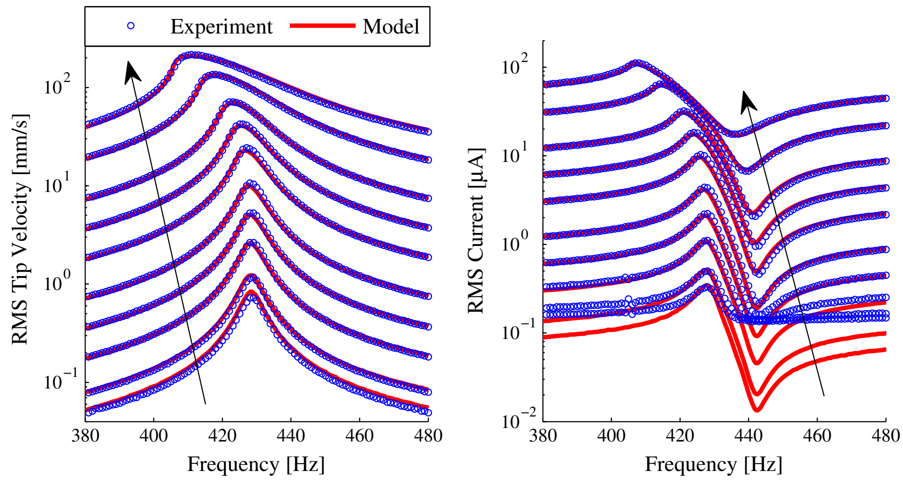

Fig. 9 RMS tip velocity and RMS actuation current responses under dynamic actuation for voltage amplitudes of 0.01, 0.02, 0.05, 0.1, 0.2, 0.5, 1, 2, 5 and 10 V. *Blue circles* represent experimental data, and *red curves* represent model predictions. *Arrows* indicate direction of increasing actuation voltage amplitude

ation, using the same parameters as in the energy harvesting tests, shows strong agreement at all voltage levels reported in Fig. 9.

6.4 Experimental backbone curve

As discussed previously in Sect. 2, quadratic and cubic nonlinearities model qualitatively different behaviors that both can be described as softening. To confirm that the type of geometrically linear, piezoelectric cantilever bimorph studied in this work is better modeled with quadratic nonlinearities than cubic nonlinearity alone, the backbone curve is found from experimental data. Shown in Fig. 10 are the open-circuit (10 MΩ) voltage responses during base acceleration tests and tip velocity responses during actuation tests for a broad range of excitation levels. For both the open-circuit energy harvesting and dynamic actuation tests, the true backbone curve is generated by fitting a second- order polynomial to the peak response points. To compare the fidelity of quadratic and cubic models for nonlinearity, purely linear and purely quadratic backbone curves are fit as well. In both open-circuit energy harvesting and dynamic actuation cases, the backbone curve is primarily linear, indicating that until very close to the safe operation limits of the cantilever, a quadratic stiffness model is satisfactory. For the open-circuit base excitation case, the purely linear backbone curve has an R^2 value of 0.988, while the purely quadratic backbone curve fits more poorly with an R^2 value of 0.926. For the dynamic actuation case, the linear backbone curve again better describes the true behavior, with R^2 values of 0.998 and 0.887 for the purely linear fit and purely

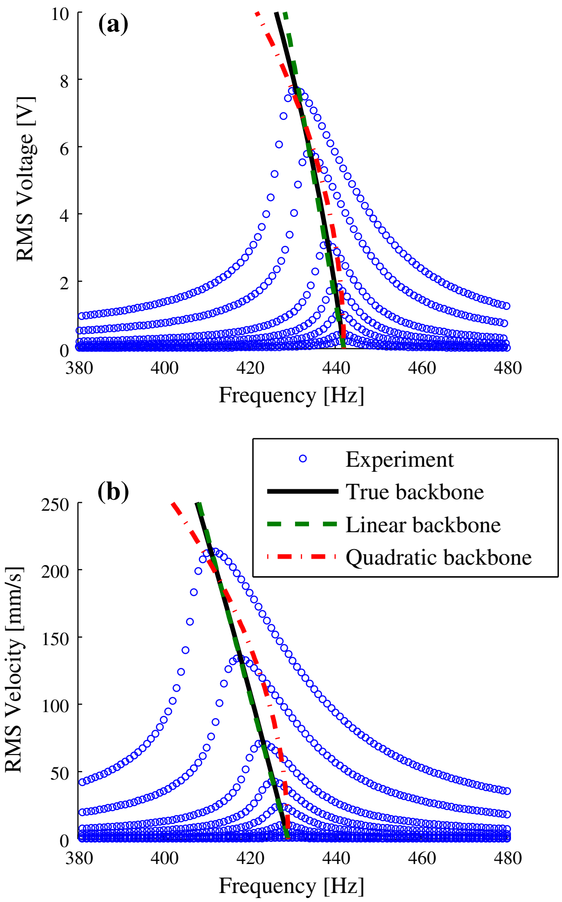

Fig. 10 Open-circuit voltage responses for various base acceleration levels (**a**) and tip velocity responses to various excitation voltage levels (**b**). Experimental data are shown by *blue circles*. Linear and purely quadratic backbone curve fits are shown by *green dashed* and *red dash-dot curves*, respectively. The best fit backbone curve with both linear and quadratic variation is shown in *black*

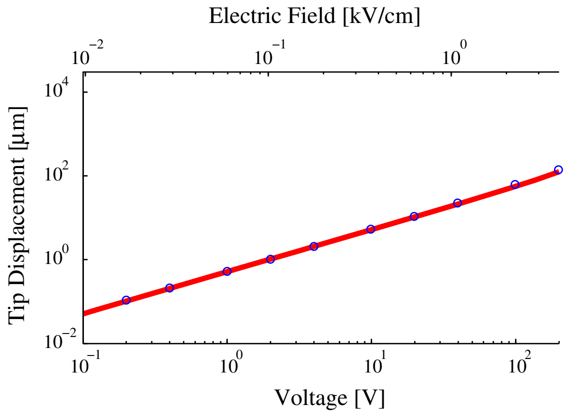

Fig. 11 Quasi-static (10 Hz) tip displacement versus actuation voltage amplitude. Experimental data are shown by *blue circles*, and model prediction is shown by the *red curve*

quadratic fit cases, respectively. Importantly, the experimental backbone curve clearly does not cross the frequency axis at a right angle, which is characteristic of a purely cubic stiffness nonlinearity. Therefore, models in which quadratic terms vanish cannot accurately model observed behavior.

6.5 Quasi-static actuation experiments

While the proposed models and analysis pertains directly to the behavior of piezoelectric bimorph cantilevers near resonance, low frequency actuation tests were conducted to evaluate the model's performance for quasi-static, high voltage actuation. Low-frequency, off-resonant excitation allows for high voltage input levels that would damage the brittle sample structurally if applied near resonance. Using the same experimental apparatus as the dynamic actuation tests, the sample cantilever was actuated with a 10 Hz harmonic voltage with amplitudes ranging from 0.2 to 200 V. The highest voltage level of 200 V results in an electric field of 3.8 kV/cm for each piezoelectric layer (still below the coercive field of 12 kV/cm, but closer in terms of the order of magnitude as compared to the previous section). Figure 11 displays the variation of tip displacement amplitude with actuation voltage amplitude. For actuation voltages of 20 V and below, the model accurately predicts the relationship between actuation voltage and displacement, which is governed by the ratio of electromechanical coupling to stiffness. For higher voltages exceeding the levels achievable in energy harvesting applications or resonant actuation, the model underpredicts the deflection. For the 200 V test, the voltage is an order of magnitude higher than in the highest resonant actuation test, while the maximum deflections observed are on the same order of magnitude (~0.1 mm). Therefore, the error is likely due to electromechanical coupling or excluded electric field nonlinearities rather than stiffness. A model that can more accurately predict both resonant and off-resonant actuation should include linear and quadratic stiffness terms and linear, quadratic, and cubic electromechanical coupling terms. High-field hysteretic effects [21] and resulting dissipation become important and should be included for excitations close to the coercive field.

7 Conclusions

An experimentally validated, nonlinear, nonconservative model has been proposed to describe the energy harvesting, sensing, and dynamic actuation behavior of soft (e.g., PZT-5A, PZT-5H) piezoelectric cantilevers for a wide (low to moderately high) range of mechanical and electrical excitation levels. A set of governing partial differential equations was derived using Hamilton's principle. Those equations were spatially discretized for the fundamental bending mode, creating a lumped parameter model to be analyzed using the method of harmonic balance. The model showed excellent agreement to extensive experimental investigation of energy harvesting and dynamic actuation over the full range of structurally safe excitation levels of the brittle PZT-5A bimorph cantilever near resonance. The agreement of the model and experiment at all excitation levels is evidence that the dominant stiffness and electromechanical coupling nonlinearity apparent in certain piezoelectric structures is quadratic in nature. The backbone curves of both energy harvesting and actuation frequency responses are reported to be dominantly of first order for a broad range of mechanical and electrical excitation levels, in agreement with the experiments. While quadratic terms vanish during the analysis of a symmetric bimorph when examining polynomial electric enthalpy expansions in strain, a modified expansion form in strain amplitude retains those quadratic terms. Therefore, nonlinear effects associated with ferroelastic softening and dissipation should be given the priority in modeling of electroelastic nonlinearities in energy harvesting, sensing, and actuation for low to moderately nonlinear response forms with electric fields well below the coercive field. It should be noted that the focus has been placed on a soft piezoelectric material (PZT-5A) in this work. Future efforts may explore hard piezoelectric bimorphs (e.g., PZT-4, PZT-8), for which the backbone curve trends may be altered due to a higher mechanical quality factor.

Acknowledgments This work was supported in part by the National Science Foundation under Grant CMMI-1254262.

Appendix: Remaining energy harvesting experiments and model validation

See Figs. 12, 13, 14 and 15.

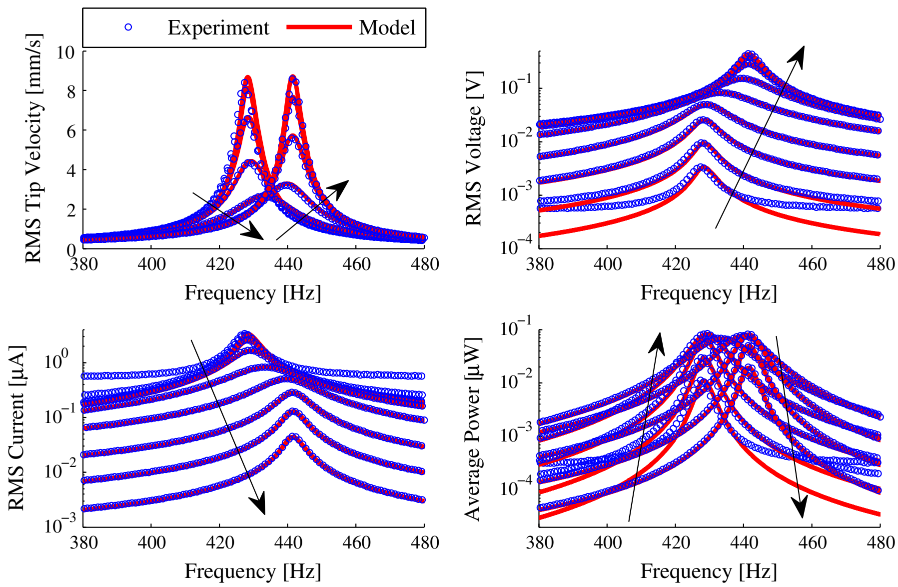

Fig. 12 Resistor sweep energy harvesting test at 0.02 g RMS base acceleration level for resistance values of 1, 3, 10, 30, 100, 300, 1, 3, and 10 MΩ. *Blue circles* represent experimental data, and *red curves* represent model predictions. *Arrows* indicate direction of increasing load resistance

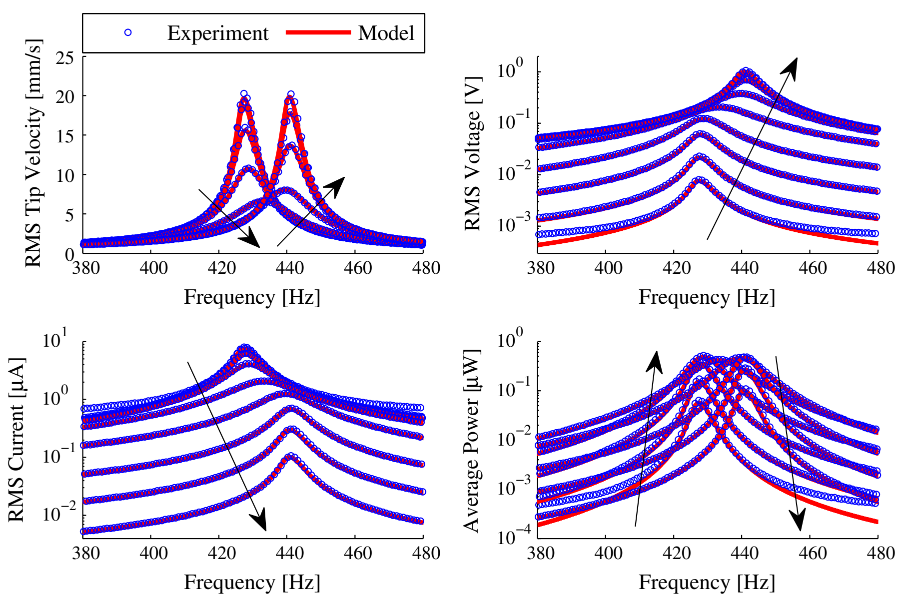

Fig. 13 Resistor sweep energy harvesting test at 0.05 g RMS base acceleration level for resistance values of 1, 3, 10, 30, 100, 300, 1, 3, and 10 MΩ. *Blue circles* represent experimental data, and *red curves* represent model predictions. *Arrows* indicate direction of increasing load resistance

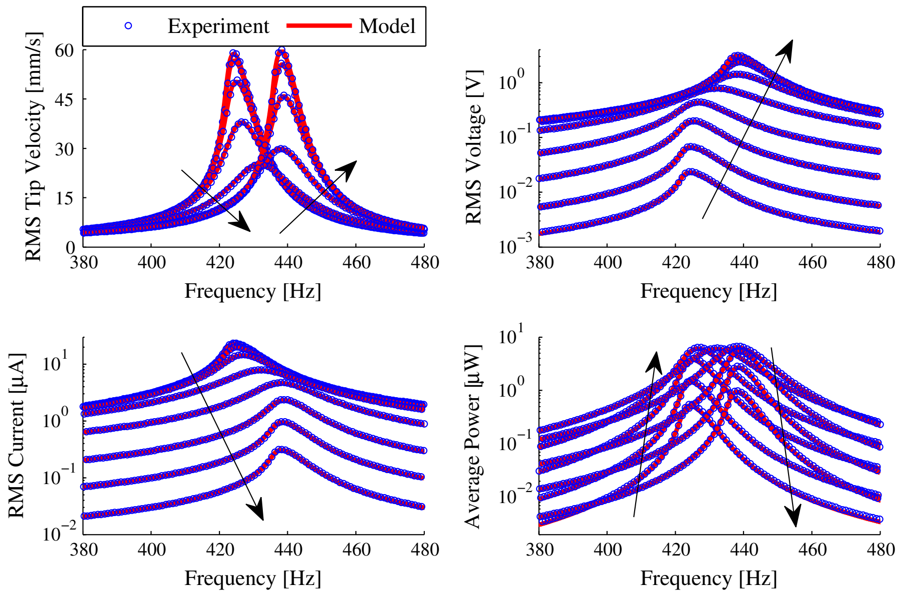

Fig. 14 Resistor sweep energy harvesting test at 0.20 g RMS base acceleration level for resistance values of 1, 3, 10, 30, 100, 300, 1, 3, and 10 MΩ. *Blue circles* represent experimental data, and *red curves* represent model predictions. *Arrows* indicate direction of increasing load resistance

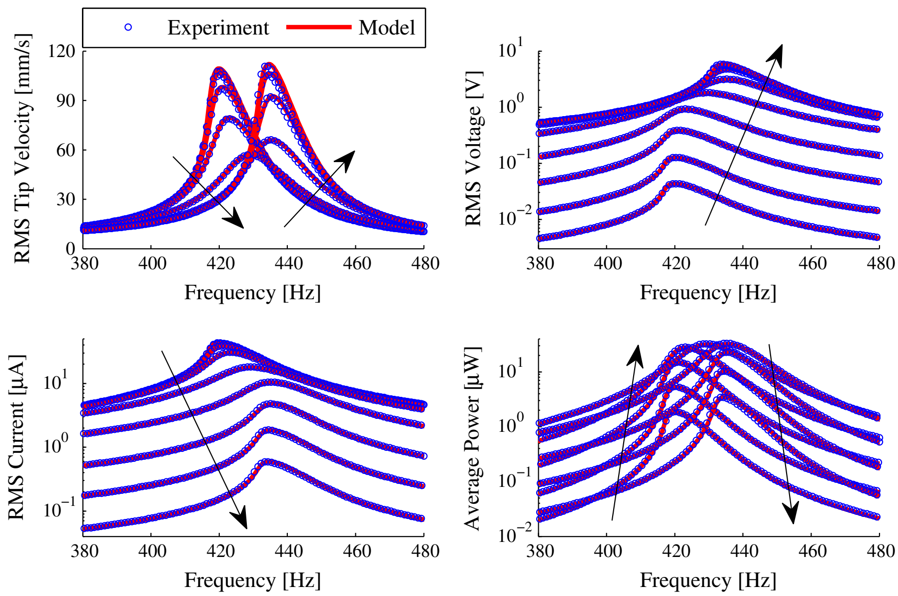

Fig. 15 Resistor sweep energy harvesting test at 0.50 g RMS base acceleration level for resistance values of 1, 3, 10, 30, 100, 300, 1, 3, and 10 MΩ. *Blue circles* represent experimental data, and *red curves* represent model predictions. *Arrows* indicate direction of increasing load resistance

References

1. Maugin, G.A.: Nonlinear Electromechanical Effects and Applications, vol. 1. World Scientific, Singapore (1985)
2. Tiersten, H.F.: Electroelastic equations for electroded thin plates subject to large driving voltages. J. Appl. Phys. **74**, 3389–3393 (1993)
3. Aurelle, N., Guyomar, D., Richard, C., Gonnard, P., Eyraud, L.: Nonlinear behavior of an ultrasonic transducer. Ultrasonics **34**, 187–191 (1996)
4. Guyomar, D., Aurelle, N., Eyraud, L.: Piezoelectric ceramics nonlinear behavior. Application to langevin transducer. J. De Physique **III**(7), 1197–1208 1997)
5. Abdelkefi, A., Nayfeh, A.H., Hajj, M.R.: Effects of nonlinear piezoelectric coupling on energy harvesters under direct excitation. Nonlinear Dyn. **67**, 1221–1232 (2011)
6. Abdelkefi, A., Nayfeh, A.H., Hajj, M.R.: Global nonlinear distributed-parameter model of parametrically excited piezoelectric energy harvesters. Nonlinear Dyn. **67**, 1147–1160 (2011)
7. Wang, Q.M., Zhang, Q.M., Xu, B.M., Liu, R.B., Cross, L.E.: Nonlinear piezoelectric behavior of ceramic bending mode actuators under strong electric fields. J. Appl. Phys. **86**, 3352–3360 (1999)
8. Albareda, A., Gonnard, P., Perrin, V., Briot, R., Guyomar, D.: Characterization of the mechanical nonlinear behavior

of piezoelectric ceramics. IEEE Trans. Ultrason. Ferroelectr. Freq. Control **47**, 844–853 (2000)
9. Priya, S., Viehland, D., Carazo, A.V., Ryu, J., Uchino, K.: High-power resonant measurements of piezoelectric materials: importance of elastic nonlinearities. J. Appl. Phys. **90**, 1469–1479 (2001)
10. Wolf, K., Gottlieb, O.: Nonlinear Dynamics of a Cantilever Beam Actuated by Piezoelectric Layers in Symmetric and Assymetric Configuration. Technion-Israel Institute of Technology, Technical Report ETR-2001-02 (2001)
11. Usher, T., Sim, A.: Nonlinear dynamics of piezoelectric high displacement actuators in cantilever mode. J. Appl. Phys. **98**, 64102 (2005)
12. Von Wagner, U., Hagedorn, P.: Piezo-beam systems subjected to weak electric field: experiments and modelling of non-linearities. J. Sound Vib. **256**, 861–872 (2002)
13. Mahmoodi, S.N., Jalili, N., Daqaq, M.F.: Modeling, nonlinear dynamics, and identification of a piezoelectrically actuated microcantilever sensor. IEEE-ASME Trans. Mechatron. **13**, 58–65 (2008)
14. Hu, Y., Xue, H., Yang, J., Jiang, Q.: Nonlinear behavior of a piezoelectric power harvester near resonance. IEEE Trans. Ultrason. Ferroelectr. Freq. Control **53**, 1387–1391 (2006)
15. Stanton, S.C., Erturk, A., Mann, B.P., Inman, D.J.: Nonlinear piezoelectricity in electroelastic energy harvesters: modeling and experimental identification. J. Appl. Phys. **108**, 74903 (2010)
16. Stanton, S.C., Erturk, A., Mann, B.P., Inman, D.J.: Resonant manifestation of intrinsic nonlinearity within electroelastic micropower generators. Appl. Phys. Lett. **97**, 254101 (2010)
17. Nayfeh, A.H., Mook, D.T.: Nonlinear Oscillations. Wiley, New York (2008)
18. Stanton, S.C., Erturk, A., Mann, B.P., Dowell, E.H., Inman, D.J.: Nonlinear nonconservative behavior and modeling of piezoelectric energy harvesters including proof mass effects. J. Intell. Mater. Syst. Struct. **23**, 183–199 (2012)
19. Goldschmidtboeing, F., Eichhorn, C., Wischke, M., Kroener, M., Woias, P.: The influence of ferroelastic hysteresis on mechanically excited PZT cantilever beams. In: Proceedings of the 11th International Workshop on Micro and Nanotechnology for Power Generation and Energy Conversion Applications, pp. 114–117 (2011)
20. Kamlah, M.: Ferroelectric and ferroelastic piezoceramics-modeling of electromechanical hysteresis phenomena. Contin. Mech. Thermodyn. **13**, 219–268 (2001)
21. Damjanovic, D.: Hysteresis in piezoelectric and ferroelectric materials. Sci. Hysteresis **3**, 337–465 (2005)
22. Smith, R.C., Seelecke, S., Dapino, M., Ounaies, Z.: A unified framework for modeling hysteresis in ferroic materials. J. Mech. Phys. Solids **54**, 46–85 (2006)
23. Crandall, S.H.: Dynamics of Mechanical and Electromechanical Systems. McGraw-Hill, New York (1968)
24. Erturk, A., Inman, D.J.: Piezoelectric Energy Harvesting. Wiley, New York (2011)
25. Dutoit, N.E., Wardle, B.L.: Experimental verification of models for microfabricated piezoelectric vibration energy harvesters. AIAA J. **45**, 1126–1137 (2007)
26. Erturk, A., Inman, D.J.: An experimentally validated bimorph cantilever model for piezoelectric energy harvesting from base excitations. Smart Mater. Struct. **18**, 025009 (2009)